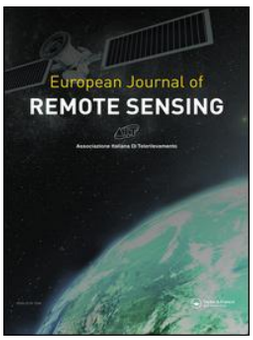

European Journal of Remote Sensing

ISSN: (Print) (Online) Journal homepage: https://www.tandfonline.com/loi/tejr20

Elevation change of Bhasan Char measured by persistent scatterer interferometry using Sentinel-1 data in a humanitarian context

Andreas Braun , Thorsten Höser & José Manuel Delgado Blasco

To cite this article: Andreas Braun , Thorsten Höser & José Manuel Delgado Blasco (2020): Elevation change of Bhasan Char measured by persistent scatterer interferometry using Sentinel-1 data in a humanitarian context, European Journal of Remote Sensing, DOI: 10.1080/22797254.2020.1789507

To link to this article: https://doi.org/10.1080/22797254.2020.1789507

Published online: 06 Jul 2020.

EUROPEAN JOURNAL OF REMOTE SENSING
https://doi.org/10.1080/22797254.2020.1789507

Taylor & Francis
Taylor & Francis Group

Elevation change of Bhasan Char measured by persistent scatterer interferometry using Sentinel-1 data in a humanitarian context

Andreas Braun [a], Thorsten Höser [b] and José Manuel Delgado Blasco [c,d]

[a]Department of Geography, University of Tübingen, Tübingen, Germany; [b]German Aerospace Center (DLR), German Remote Sensing Data Center (DFD), Oberpfaffenhofen, Germany; [c]RHEA Group c/o ESA/ESRIN, Frascati, Italy; [d]Grupo De Investigación Microgeodesia Jaén (PAIDI RNM-282), Universidad De Jaén, Jaén, Spain;

ABSTRACT

This study investigates the elevation changes for the island of Bhasan Char, located in the Bay of Bengal, which was selected for the relocation of around 100,000 refugees of the Rohingya minority which were forced to leave their homes in Myanmar. Eighty-nine Sentinel-1 products were analysed using persistent scatterer interferometry (PSI) beginning August 2016 through September 2019, divided into three periods of one year to reduce the impact of temporal decorrelation. The findings indicate that the island is a recent landform which underlies naturally induced surface changes with velocities of up to ±20 mm per year. Additional displacement is probably caused by heavy construction loads since early 2018, although we found no statistical evidence for this. The main built-up area shows stable behaviour during the analysed period, but there are significant changes along the coasts and artificial embankments of the island, and within one separate settlement in the north. The moist surface conditions and strong monsoonal rains complicated the proper retrieval of stable trends, but the sum of findings supports the assumption that the island underlies strong morphologic dynamics which put the people to be relocated at additional risk. Its suitability for construction has to be investigated in further studies.

ARTICLE HISTORY
Received 4 November 2019
Revised 11 May 2020
Accepted 26 June 2020

KEYWORDS
Persistent scatterer interferometry; radar remote sensing; humanitarian aid; time-series analysis; surface displacement; stamps; Sentinel-1; PS InSAR

Background and aims

Methods of earth observation and spaceborne remote sensing have significantly contributed to our understanding of the earth and the processes occurring on its surface. It is especially a valuable tool whenever an area of interest is too large to conduct a field survey or when it is impracticable or even dangerous to access it. For this reason, humanitarian work has become increasingly interested in the field of remote sensing for various applications. Humanitarian organizations not only benefit from satellite images as a constant and objective source of information but also because spatio-temporal patterns, derived by experts from complex data, can be interpreted by a wide audience to communicate crisis situations (Lang et al., 2015, 2019). Such information is required to make planning decisions regarding the management of settlements for people in need, their supply of goods and medical services, their protection against natural hazards, and the sustainable investment of future funds (Verjee, 2007). It was already demonstrated in the beginning of the 20th century how satellite imagery can be used for the mapping of refugee camps and the monitoring of their surroundings (Bjorgo, 2000; Giada et al., 2003; Lodhi et al., 1998). With technological progress, the spatial resolution of the sensors increased, and new methods were developed which helped to automate such tasks. Among the most important were the object-based analysis of very high-resolution (VHR) images of refugee camps (Hagenlocher et al., 2012; Lang et al., 2010; Spröhnle et al., 2017), methods of template matching and machine learning (Ghorbanzadeh et al., 2018; Laneve et al., 2006; Quinn et al., 2018; Tiede et al., 2017), and studies based on synthetic aperture radar (SAR) images (Amitrano et al., 2013; Braun, 2018; Braun et al., 2019). However, most of the approaches deal with the observation of land use and landcover as well as their socio-economic implications.

The spatio-temporal dimensions of armed conflicts are analysed by several studies, for example, by using fire occurrence derived from the MODIS mission as a proxy for street fights and burnings to retrospectively track the outbreak of violence after the national elections in December 2007 in Kenya (Anderson & Lochery, 2008). Other studies make use of night-time data of the DMSP-OLS mission as an indicator for the presence of civilization and functioning infrastructures to evaluate the progress of the Syrian Civil War (Li & Li, 2014) as well as wars in the Caucasus regions of Russia and Georgia (Witmer & O'Loughlin, 2011). A number of publications deal with the detection of damaged huts and villages based on VHR optical imagery from QuickBird (Sulik & Edwards, 2010),

CONTACT Andreas Braun an.braun@uni-tuebingen.de Tübingen, 72072

Ikonos (O'Connell & Young, 2014), and WorldView (Knoth & Pebesma, 2017) during the Darfur crisis in Sudan, also some of them are also based on changes in surface elevations, for example, as presented by d'Oleire-Oltmanns, S., Tiede, D., Krauß, T. and Wendt, L (2018) who derived damages in the city of Mosul during the Syrian Civil War based on stereo-analysis of Pléiades imagery. Furthermore, notable in this context are studies listed by Marx and Goward (2013) who demonstrate the use of satellite images to identify human rights violations by determining the capacity of prison camps in North Korea, and mass graves during the Srebrenica massacre in Bosnia.

Compared with the previously outlined research in the field of humanitarian remote sensing, this study deals with rather long-term aftermaths of forced displacement, as the marginalisation of the Rohingya population in Burma reaches back into the colonial era of the 19th century. (Milton et al., 2017). As of today, they are considered "resident foreigners", thus are not given citizen rights and often subject to discrimination, violence and other human rights violations (Ullah, 2011). During the last two decades over one million Rohingyas fled into the neighbouring country of Bangladesh which is obligated to ensure their protection as a country of first asylum. However, as the country's settlement areas and resources are limited, and the refugee camps in Cox's Bazar are prone to recruitment of militant groups, security concerns were raised which consider this humanitarian crisis a threat to Bangladesh's internal stability (Bashar, 2017; Rahman, 2010). In addition to the massive expansion of the Kutupalong refugee camp, the government of Bangladesh announced plans to relocate about 100,000 Rohingya refugees to the island of Bhasan Char in the Bay of Bengal (Martin et al., 2018). These plans have been severely criticized by humanitarian organizations and governments because of concerns regarding the island's security during high tides and monsoonal rains plus the spatial and social isolation of the resettled people on this yet uninhabited islandisland (Guhathakurta, 2017)

But while studies on the energetic power provision (Sunny et al., 2019) and even the touristic potential (Nasrin, 2019) of the sandbanks in the Gulf of Bengal were already conducted, no publications on their suitability for heavy construction or their likelihood of being flooded exist so far.

However, as demonstrated by Braun and Hochschild (2018) and Lang et al. (2019), the extent of the island underlies strong seasonal dynamics, most likely related to sea surface levels, and that the island is a very recent landform which has not existed before the year 2010. As it was formed from silts washed down from the Himalayan mountains, it is still undergoing considerable surface changes and natural consolidation processes (Bandyopadhyay et al., 2014). However, independent field measurements on the stability of this island are not available.

A spaceborne method to quantify the change of surface elevations over a longer time is persistent scatterer interferometry (PSI; see section 2.3.1). This multi-temporal technique is able to measure deformation rates at a millimetre scale and was successfully applied to investigate land subsidence phenomena induced by anthropogenic and natural events in numerous studies (Crosetto, Monserrat, Cuevas-González et al., 2016). However, most of these studies focus on mainland or coastal urban areas, as shortly presented in the following.

On the one hand, there are studies focussing the potential drivers of subsidence: Aly et al. (2012) analysed ERS data of the Nile Delta using PSI and report regionally heterogenous subsidence patterns, underlying cyclic deformations rates due to groundwater extraction. Human settlements and their building load were discerned as a drivera driver for subsidence due to an accelerated soil consolidation process from latest urbanization as investigated by Solari et al. (2016) in Pisa, and Hu et al. (2019) in Shenzhen and Hong Kong. A variety of processes caused ground subsidence in the Italian metropolitan areas of Rome (Delgado Blasco et al., 2019), Venice (Dehghani et al., 2013; Teatini et al., 2012), and Napoli (Terranova et al., 2015). A combination of two triggers, groundwater extraction and high building volumes, caused subsidence in Beijing (Yang et al., 2018), as well as construction load on reclaimed land in combination with subterranean oil storage tanks, investigated by J. S. Kim et al. (2007) for a coastal harbour peninsula of Incheon city in Indonesia.

On the other hand, there are also studies which concentrate on the aftermaths and risks of land subsidence, which can not only cause damage to infrastructures and settlements but also increase the risk of floods and permanent loss of land, especially when combined with sea level rise. Consequences of current and future urban subsidence rates associated with aquifer systems within the South Korean harbour city Mokpo were analysed and predicted by S.-W. Kim et al. (2010) based on 23 images of JERS-1 acquired between 1992 and 1998. Abidin et al. (2013) measure the effect of soil compaction in the coastal area of the capital of Java based on GPS and InSAR measurements and relate them to the spatial distribution of different impacts, such as coastal flooding, cracks in buildings, tilting houses and damages to infrastructures, such as roads or bridges. And also Osmanoğlu et al. (2011) present the damaging effects of subsidence on urban subway lines and the Metropolitan Cathedral in iin Mexico City. In a large-scale application, Cian et al. (2019) investigated the risks of urban flooding using an automated PSI approach with a focus on freely available data and

tools on 18 coastal cities in Sub-Saharan Africa, detecting subsidence in 17 of them.

As indicated above, all these studies analyse existing cities on the mainland. Only few studies deal with deformations of non-urban coastal environments. In this context, PSI is predominantly used for the monitoring of volcanoes (Schaefer et al., 2019). Seidel et al. (2016) investigated coastal subsidence along the coast of Northern Germany with PSI, but struggle to retrieve reliable data outside the concrete man-made structures on the dykes. The same problem is reported by Da Lio and Tosi (2018) who measure coastal deformation in urban areas North-eastern Italy: While urban areas provide enough solid structures for reliable measurements, the deformations detected for an offshore sandbank were statistically insignificant because of a low density of suitable radar targets.

Accordingly, to partially close this research gap, the aims and innovations of this study are

1.to present a PSI approach to determine the long-term stability of the Bhasan Char sandbank,

2.to test for an impact of the buildings which were constructed in 2018,

3.to demonstrate the use of Sentinel-1 data and PSI for humanitarian advocacy and risk assessment, and

4.to present and discuss results and shortcomings to define the research need for future studies.

It shall help to clarify if the island undergoes significant changes and if these are related to the construction activities. However, in order to protect the people who are affected by the envisaged relocation, and to prevent potential misuse of the findings, this study concentrates on the physical characterisation of this island and will not give any recommendations on its suitability for habitation.

Data and methods

Figure 1 shows the overall design of the study which will be explained at more detail in the next sections. The box on the left side helps to follow the data processing in section 2.3.2. Additionally, the box on the right side lists the steps for the derivation of surface displacement as described in section 2.3.3.

Study *area*

Bhasan Char is an uninhabited island in the Bay of Bengal which lies approximately 20 20 km off the coast of Bangladesh (Figure 2). The land area ranges about 7.5 7.5 km in a north/south and east/west direction but is subject to large variations. As found by Braun and Hochschild (2018), the land area varied between 39 km^2 and 76 km^2 during the past five year5 years. Studies of Islam et al. (2019) also report an invariant alternation between erosion and accretion during the last decade, but with an overall gradual movement of the island in southwest direction. At the current point, it is not clear yet if the decreasing trend of land mass of Bhasan Char, as it is indicated by Figure 2, will continue or if the island will stabilize like other sand banks in this bay replenished by sediments washed from the waters of the Ganges-Brahmaputra-Meghna river system (Banerjee, 2020). The first evidence of built-up structures (embankments, channels, first buildings) was found in February 2018 based on visual inspection

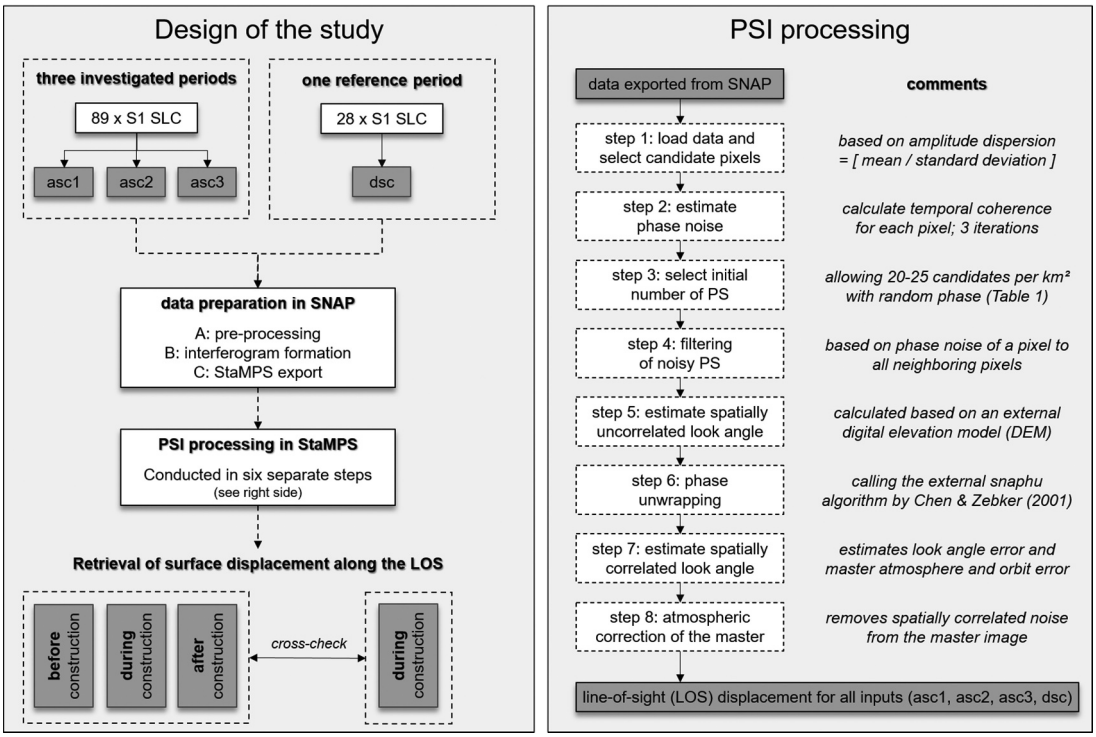

Figure 1. Design of the proposed study (left) and order of PSI processing (right).

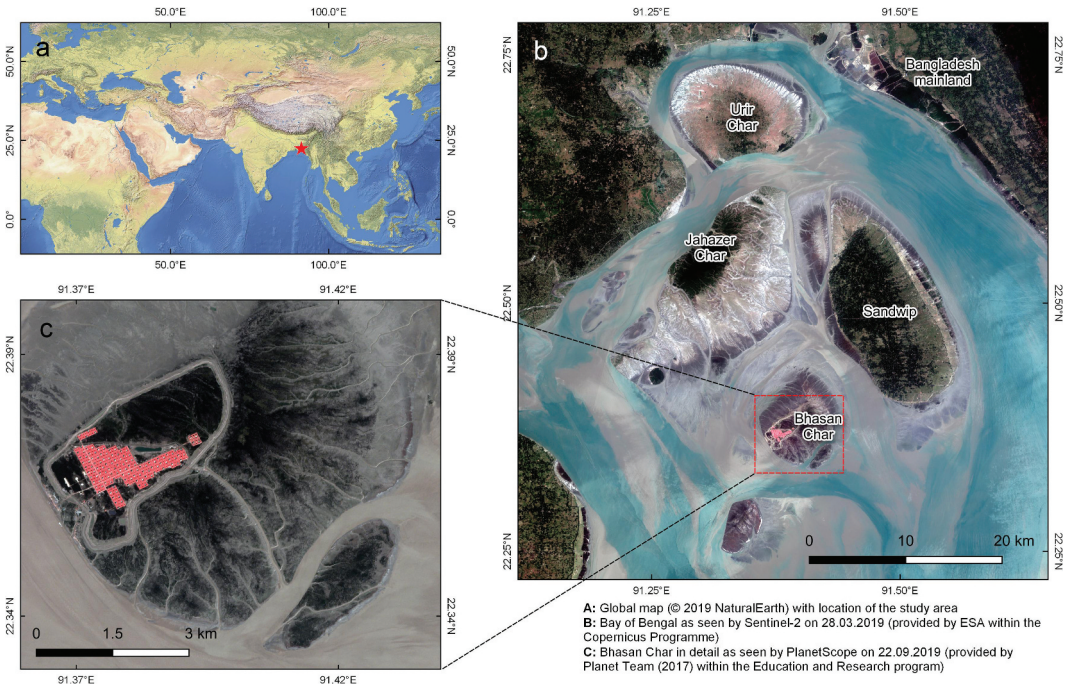

Figure 2. Study area for the analysis of surface variations of Bhasan Char. A: Location at the global scale. B: Location of Bhasan Char in the Bay of Bengal. C: Satellite image from September 2019 documenting the stage of construction.

of Sentinel-2 time-series. The island itself consists of wet and muddy sediments of rippled texture with almost no natural vegetation cover, besides sparse grass and shrubs, and reportedly the degree of water saturation is the outcome of the tidal movements in the bay (Ul Haque, 2011).

The temporal dynamics of the land masses and its coverage are impressively demonstrated in Figure 3 which compares colour composites of Sentinel-1 back-scatter intensity of various years. They were averaged based on all available images per year acquired in descending mode (2014: n = 3, 2015: n = 11, 2016: n = 14, 2017: n = 36, 2018: n = 53, 2019: n = 14). The figure not only shows how the construction of the embankments, the circular drainage channel, and the buildings changed the nature of the island, but also that large parts of the land mass are regularly flooded. These are the shores along the northern coast which are darker in the temporal average, because of their regular flooding, but also the runoff channels which are cutting deep into the landmass from the south and southeast.

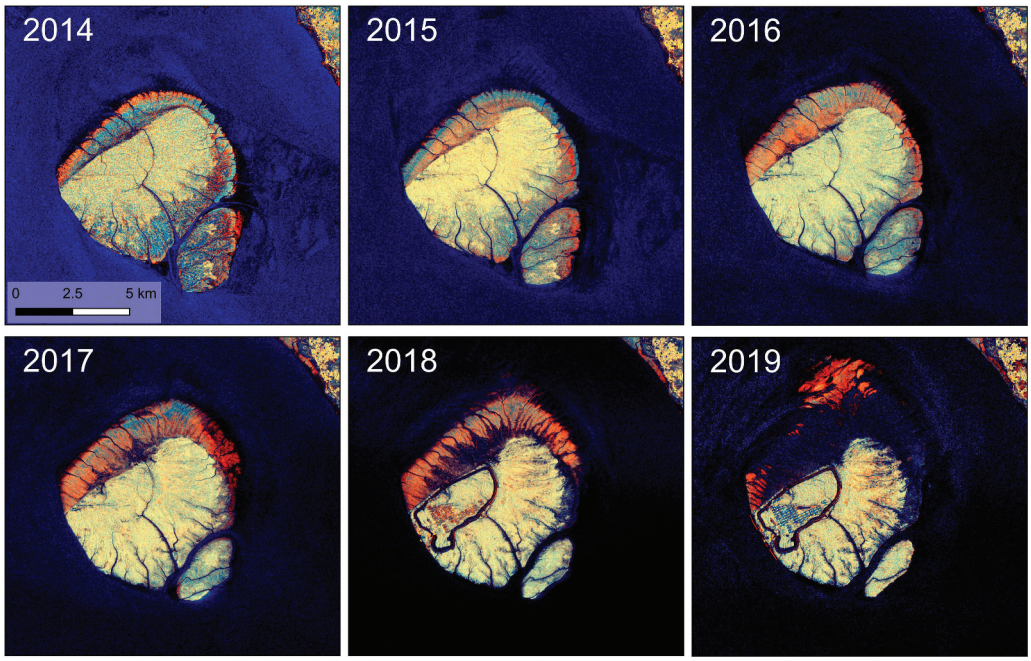

Figure 3. Backscatter intensity of Bhasan Char displayed as polarimetric colour composites (red = VV, green = VH, blue = VH-VV).

Satellite data

To analyse the surface variations on the island, 89 Sentinel-1 single look complex (SLC) products acquired in Interferometric Wide-Swath (IW) mode between August 2016 and September 2019 in descending direction (path 114) were used in this study. As the number of persistent scatterers which can potentially be identified from the time series decreases in the course of time, the investigated time was divided into three intervals of one-year length as displayed in green, blue, and orange in Figure 4. They were selected to represent periods before (08/2016 – 08/2017; asc1), during (09/2017 – 08/2018; asc2) and after the construction works (09/2018 – 09/2019; asc3) have started in early 2018.

In an ideal case, surface displacement measured along the line-of-sight (LOS) derived from ascending and descending data is combined to determine the absolute vertical surface motion, such as recently conducted by Delgado Blasco et al. (2019). Unfortunately, no descending images are available in the study area between January and August 2019, and only at large intervals before November 2017. For this reason, a one-year period of 28 images acquired in descending direction (path 77) were used as a reference dataset (01/2018 – 01/2019; dsc).

Each of the four analysed time-series (asc1, asc2, asc3, dsc) requires the selection of one master image which will be used for co-registration with each slave image for the computation of an interferogram (section 2.3). The master images of each period were selected by minimizing the overall decorrelation of the spatial and temporal baseline as well as the differences in Doppler centroid (Figure 3, triangles). Besides the temporal aspect, the perpendicular baseline of the master image to all slaves needs to be balanced. Figure 5 shows the baseline charts for all four investigated periods with the master image at the origin and the relative positions of all used slave images. Each line stands for an image pair used to compute an interferogram as described in the next section.

Calculation of surface displacement

Persistent scatterer radar interferometry

Differential SAR interferometry (DInSAR), as a traditional method to measure surface deformations from space, investigates the interferometric phase ϕ of two complex SAR acquisitions. As described in Equation 1, ϕ mainly results from different signal contributions, namely topographic phase ϕ_{topo}, the flat-earth phase ϕ_{flat}, the look angle error ϕ_{lae}, the phase contribution due to surface displacement occurred between the two acquisitions ϕ_{disp}, the atmospheric phase screening ϕ_{asp}, and other processing-induced factors ϕ_{noise}.

$$\phi=\phi_{topo}+\phi_{flat}+\phi_{lae}+\phi_{disp}+\phi_{aps}+\phi_{noise} \quad (1)$$

Accordingly, ϕ_{disp} can be retrieved by modelling or estimating all other phase contributions and subtracting them from the interferometric phase ϕ (Berardino et al., 2002; A. Ferretti et al., 2007; Hanssen, 2001).

However, traditional DInSAR approaches are limited in cases of non-linear deformation rates and observations over longer time intervals which cause decorrelation of the phase information (Villasenor & Zebker, 1992). Especially the sandy and moist conditions of Bhasan Char (see section 2.1) introduce errors and prevent a reliable exploitation of the displacement phase contribution ϕ_{disp}. To characterize non-linear and fine-scaled deformation rates over a longer time persistent scatterer interferometry (PSI) was developed which makes use of entire time-series of images and their relative phase differences (A. Ferretti et al., 2000, 2001). Its application for this case is described in the following.

Pre-processing

This work used the snap2stamps open sourcopen-source package, which was developed by Delgado Blasco and Foumelis (2018) to facilitate the automated interferometric processing of Sentinel-1 data forming single master DInSAR products. It consists of python scripts which systematically call the Graph Processing Tool (GPT) of the Sentinel-1 Toolbox distributed within the ESA SentiNel Application Platform (SNAP, Veci et al., 2014) to execute predefined graphs for the creation of single master inferferograminterferograms. The first version of this package was released in July 2018 Foumelis et al. (2018), allowing the creation of stacks of single master interferograms in batch

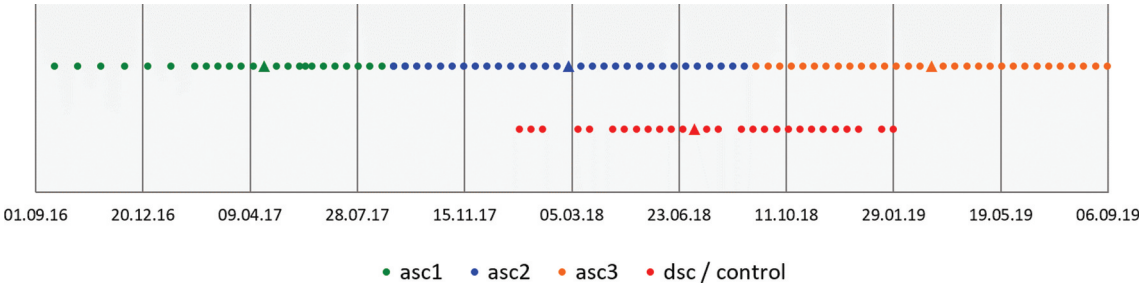

Figure 4. Temporal distribution of the analysed Sentinel-1 images for the three three investigated periods in ascending direction (asc, blue) and for the reference period in descending direction (dsc, red). The master images are represented as triangles.

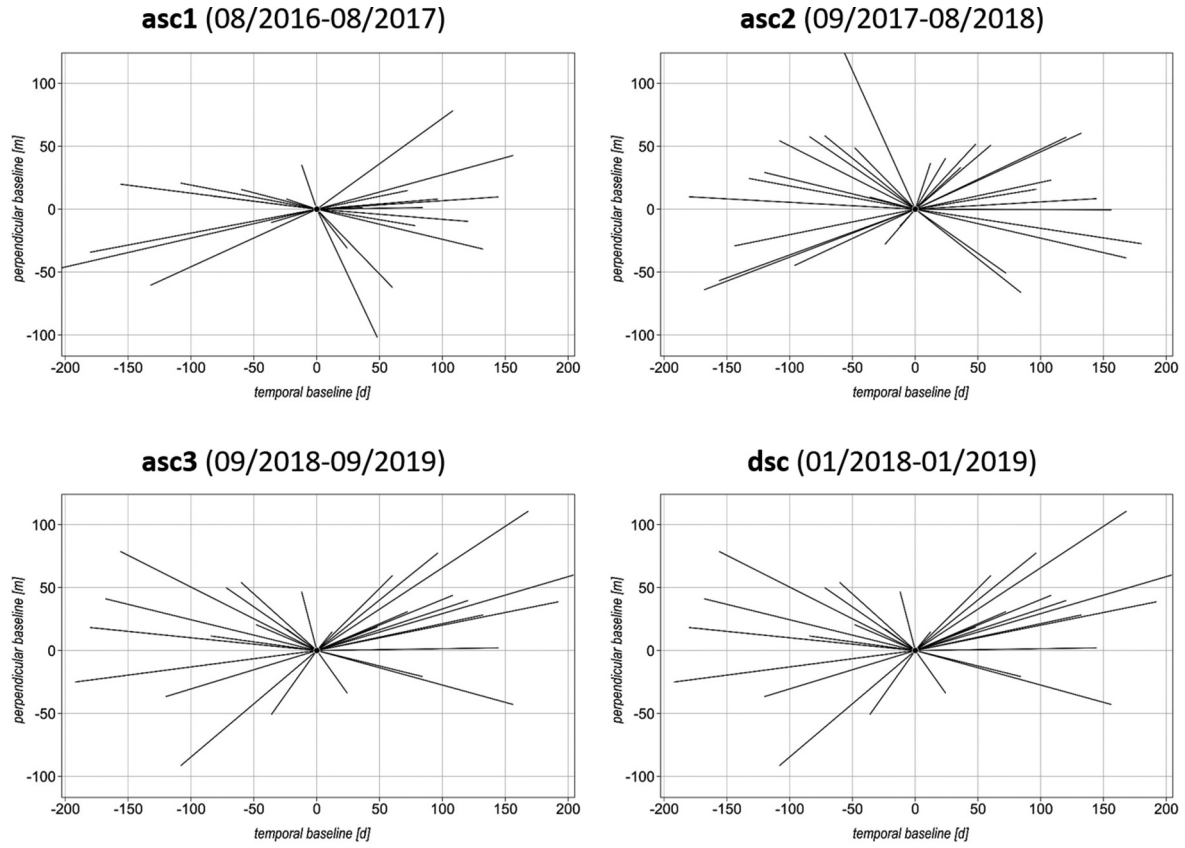

Figure 5. Baseline charts for the four periods defined in this study. Satellite positions and acquisition dates are displayed relatively to the master.

mode. The snap2stamps package is freely available via Zenodo (Delgado Blasco & Foumelis, 2018). Latest versions of the scripts (not verified by the developing team) can also be found on GitHub (Delgado Blasco, 2019).

The preparation of DInSAR products which are fully compatible with the StaMPS PSI processing is mainly based on three parts (Figure 6). In a first step (Part A), the master image of each period is prepared by selecting the required sub-swath, bursts of the TOPS product (Grandin, 2015), and orbit information with an accuracy of 5 cm is added as provided by the Payload Data Ground Segment (PDGS, 2020). This allows the subsequent co-registration with each of the slave images of each period and the formation of an interferogram in Part B. As the island only reaches a few meters above the sea level and currently no openly available digital elevation model is available which precisely describes its topography, no topographic phase removal was applied and ϕ_{topo} was assumed zero. This assumption is supported by the fact that the area suffers continuous changes during the analysed period (Figure 3). As the orbital tube of Sentinel-1 is narrow compared to other sensors (mostly smaller 100 meters), the effect of the residual topographic phase can be neglected (Crosetto, Monserrat, Devanthéryet al., 2016). Once the co-registered products and the interferograms were computed for every pair shown in the baseline plots in Figure 5, all data were exported including information on latitude and longitude (Part C).

Data analysis

The time-series analysis of the interferometric products was conducted with libraries of the Stanford Method for Persistent Scatterers (StaMPS, v4.1b) Multi-Temporal InSAR (MTI) developed by A. Hooper et al. (2012). The processing is based on a series of steps (Figure 1, right side) which will be shortly introduced in the following, to highlight when standard settings of parameters were adjusted within the valid range as defined in the manual (A. Hooper et al., 2018) and by Hooper (2018). The most important parameters are summarized in Table 1. It shows that some of the parameters had to be set differently for the four periods in order to get PS densities between 100 and 300 PS per square kilometre [PS/km^2] over the island for the ascending periods. These numbers are suggested by Colesanti et al. (2003) for the reliable description of millimetric deformation phenomena.

In a first step, pixels with a stable signal over a longer investigated period are identified based on their amplitude dispersion (ratio of the temporal amplitude standard deviation divided by the temporal mean). These candidate pixels contain a persistent radar target whose signal dominates all other random phase signals, thus granting a stable phase return over

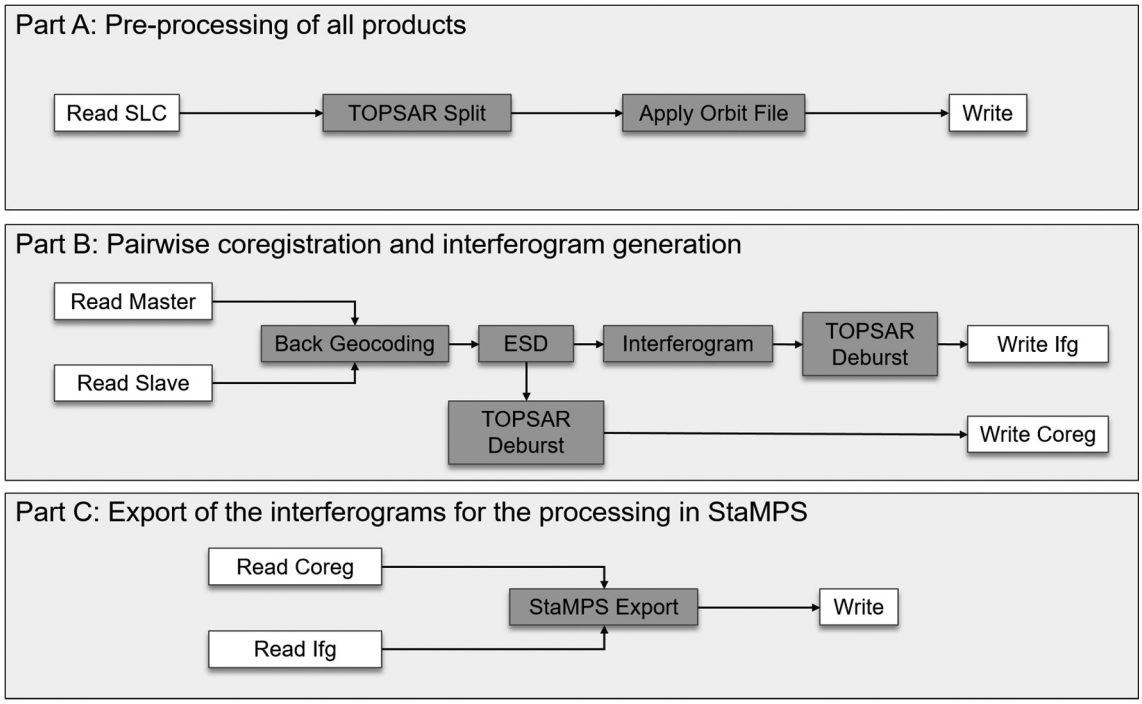

Figure 6. Pre-processing of the data using the snap2stamps package.

Table 1. Relevant parameters used for the multi-temporal processing of interferometric Sentinel-1 time-series products, and stepwise localisation of usable PS (italic).

	period			
parameter	asc1	asc2	asc3	dsc
number of Sentinel-1 images	26	31	30	28
maximum amplitude dispersion	0.42	0.42	0.42	0.42
initial number of PS candidate pixels	*76,523*	*55,118*	*73,453*	*172,153*
size of CLAP filter kernel	32	32	32	32
maximum density of random phase pixels per km^2	25	25	20	25
selected number of actual PS	*9,535*	*14,064*	*34,745*	*12,921*
standard deviation threshold (weeding)	1.75	1.75	1.00	1.00
remaining PS after dropping noisy pixels	*6,911*	*9,251*	*17,512*	*7,704*
final density [PS/km^2] over the island	*135*	*194*	*298*	*79*
estimation of a phase ramp for each interferogram	yes	yes	yes	yes
size of the temporal low-pass filter in days	60	60	60	60
reference pixel	all	all	all	91.49 22.43 (100 m)

a longer series of interferograms (Crosetto, Monserrat, Cuevas-González et al., 2016). After intensive phase filtering, as it was described by A. Hooper et al. (2007) and A. Hooper et al. (2012), the ϕ_{disp} of those selected pixels is then used to derive reliable displacement time series down to sub-wavelength magnitude of the imaging sensor. Because the island had no artificial structures before 2018, it contains only a few pixels with constant amplitude information. Hence, for the preparation of all products which were exported from SNAP (section 2.3), the threshold of the amplitude dispersion was raised from 0.4 to 0.42. This increases the number of initial persistent scatter candidates at the beginning of the processing.

In the second step, the phase noise characteristics of each pixel are estimated within an iterative process. Phase noise arises when different scattering mechanisms within one pixel contribute to its phase (A. Hooper et al., 2012). By repeatedly applying a combined low-pass and adaptive phase filter (CLAP, A. Hooper et al., 2007) with a kernel size of 32 pixels, and estimating the spatially uncorrelated DEM error, the temporal coherence of a pixel is derived as a measure for its suitability to serve as a persistent scatterer (PS).

In the third step, a first selection of PS is made based on the noise characteristics of the pixels. To maintain a minimum coverage of PS also in low coherence areas, a percentage of 25 random (non-PS) points per square kilometre is allowed. From this selection, those PS are removed in the fourth step which exceed the maximum allowed standard deviation of the phase noise to all neighbouring pixels. In order to match the more natural and unstable surface without clear dominant scatterers of the island in asc1 and asc2, during the early phase of the forming of the island, the threshold for the maximum allowed standard deviation was increased from 1.0 to 1.75 to gain a sufficient PS density to derive a constant displacement signal over the island. After this step, most pixels over water areas were removed from the analysis.

In the fifth step, the phase of each pixel is corrected for spatially uncorrelated look angle ϕ_{lae1} based on the Shuttle Radar Topography Mission (SRTM)digital elevation model (DEM). This interferometric phase is then

converted into an unambiguous phase surface in the sixth step, based on the statistical-cost network-flow phase-unwrapping algorithm (SNAPHU) developed by Chen and Zebker (2001).

In the seventh step, errors resulting from the spatially correlated look angle ϕ_{lae2} (SCLA) are calculated and removed from the data. However, as a flat surface with minor elevation is expected, the main intention of this step is the estimation of phase ramps of each interferogram which can be introduced by inaccurate orbit data of the single scenes leading false estimations on the perpendicular baselines. These phase ramps are estimated in this step so they can be removed from the later displacement results. In the eighth and last step, the contribution of atmospheric disturbances due to differences in the atmospheric phase screen (APS) is minimized by a temporal low-pass filter over time. As the length of each period is only one year, the size of the filter window was reduced to 60 days (contrary to the standard setting of 365 days). Compared to other approaches , this technique is rathersimple and does not allow to preserve non-linear deformation rates from the filter process (A. Hooper et al., 2012), but it reduces local noise to a noticeable degree.

As the resulting displacement is a relative measure, a reference area is required whose height is used to serve as zero displacement. If no reliable area is available in the image, the reference height reference value is set to the mean value of all extracted pixels.

Results and discussion

Reference period

To get a first estimate about the reliability of the approach, the descending period (dsc) from 01/2018 to 01/2019 was calculated which includes parts of the mainland of Bangladesh as a reference area for mostly stable surface conditions. Figure 7 shows the average displacement along the line of sight (LOS) of the sensor in millimetres per year. It demonstrates that there is massive variation within the surface velocities on the island, ranging between −40 and +40 mm/a, while the conditions on the mainland are comparably stable and mainly ranging between −10 and +10 mm/a. The figure gives an indication of the amount of noise remaining in the data after the processing of persistent scatterers. The little variation over the mainland hypothesises that the patterns observed over the island are not caused by processing errors or signal noise. Yet, it raises the question for the actual reasons of these differences between mainland and island, which could be caused by geologic activities (Talwani et al., 2016), ocean currents (Kolla et al., 1976) or tidal sedimentology (Reynaud & Dalrymple, 2012).

Looking at the standard variation of the surface variation (based on displacement calculated for all 28 images) a similar image is depicted: Figure 8 shows that values of the mainland are temporally constant and largely lie below 4 mm/a, while the displacement of the PS of the island undergundergoes larger temporal variations, thus indicating higher surface dynamics. The examples presented furthermore show that the segment periods of one-year provide feasible results with a sufficient density of usable PS. Yet, as shown in Table 1, the number of available PS can strongly differ for the periods.

Long-term displacement

Figure 9 shows surface velocity maps for all three investigated periods. Several things can be stated here: Firstly, the density of pixels over water areas is at an acceptably low level. This confirms that the adjustments of the parameters to reduce noisy and random pixels described in section 2.4 were largely successful. The first period (asc1) has some more pixels in the shallow water areas in the north of the island which have been continuously removed in

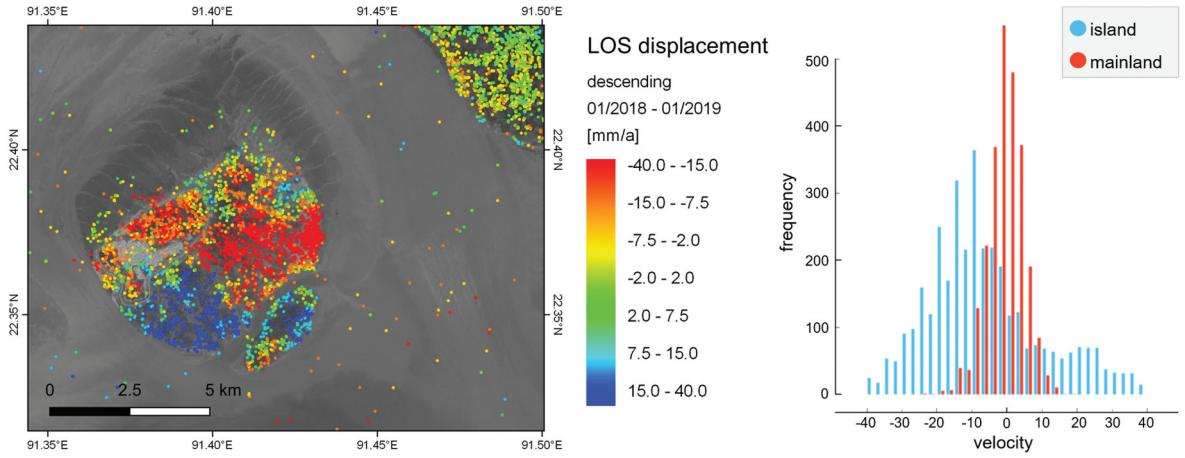

Figure 7. Spatial distribution (left) and histogram (right) of LOS displacement for period dsc (01/2018 – 01/2019) for Bhasan Char and Bangladesh's mainland.

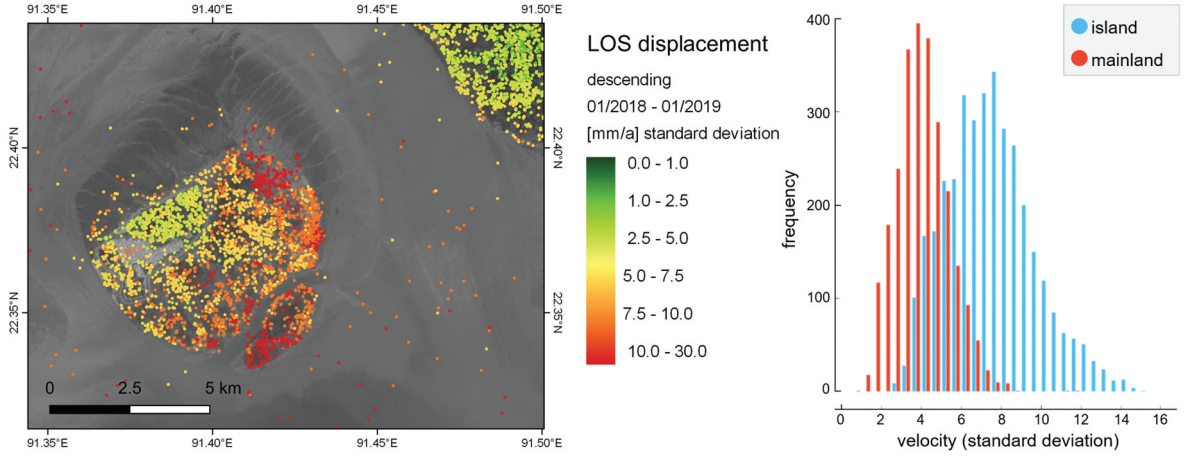

Figure 8. Standard deviation of LOS displacement for period dsc (01/2018 – 01/2019) for Bhasan Char.

favour of the flood embankment and discharge channels as it wais shown in Figure 3.

The overall patterns of the three periods are indifferent as expected. As there was no human activity before 2018, there is a comparably uniform spatial distribution of points. However, the velocities already show a large spatial variation which cannot be assigned to any anthropogenic impact. This supports the fact that the island is a very recent landform and indicates that it still experiences considerable surface dynamics, for example, caused by soil compaction, water intrusion, and coastal erosion as well as coastal accretion which are reportedly high in this area (Uddin et al., 2014). Looking at Table 1, the first

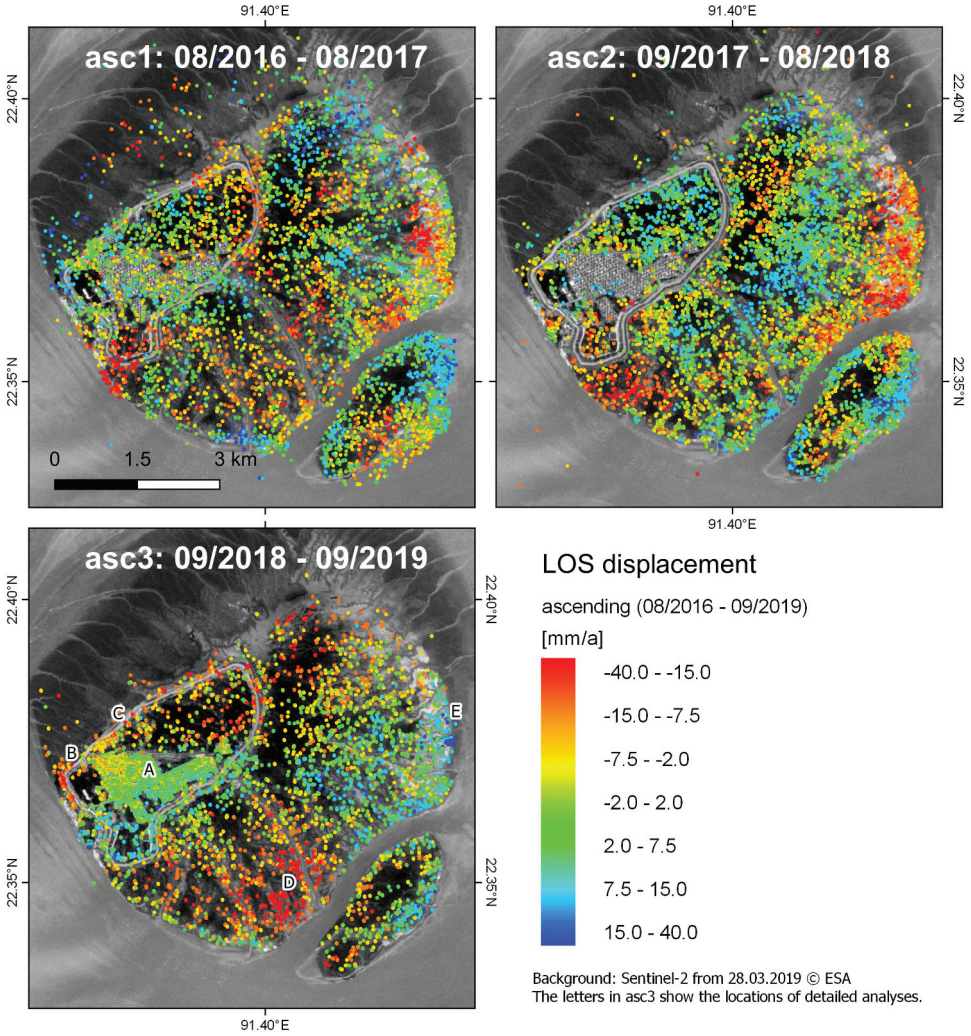

Figure 9. Spatial distribution LOS displacement for the three investigated periods.

period resulted in the smallest amount of usable PS (n = 6,911) which also indicates that there are only few radar targets with constant amplitude or phase information. Most strikingly there are two areas of strong subsidence in the southwest and the east, and two areas of elevation gain in the north and southeast of Bhasan Char.

The parts of the island which were under construction during the second period (asc2) expectedly are mostly devoid of any persistent scatterer which could be analysed. Especially the flood embankment around the construction areas and the buildings which were successively put up starting in February 2018 did not yield in any PS because their scattering mechanisms changed during the construction work which increased their amplitude dispersion. Accordingly, they were not selected as initial PS candidates in the first processing step (Figure 1, right side). During this second period, the area under subsidence in the southwest is even more pronounced than in the first period.

The third period (asc3) shows the highest PS density (298 PS/km^2), which can be mostly explained by the higher presence of stable scatterers resulting from the high level of human activity. The built-up area now has the densest distribution of PS (shown at more detail in Figure 10), because the buildings are mostly made from metal and concrete and serve as strong radar targets (marked in the map by the letter A). Different from the first two periods, there are less PS in the centre of the island, maybe because it also underwent anthropogenically induced changes. Three new hot-spots of elevation changes can be identified: Considerable subsidence along the embankment and construction area in the northwest of the built-up area (marked by B and C in Figure 9, also shown in Figure 10), subsidence in the south (marked by D), and elevation gain in the east of the island (marked by E). These will be analysed in the next section.

Figure 9 shows the distribution of PS over the built-up areas after the construction works were finished (asc3). They are predominantly characterized by stable displacement values, indicating only minor contribution of noisy pixels. However, as indicated above, the small disjointed construction area in the north (C) shows some subsidence trends, as well as the outer embankment in the west (B). The figure impressively demonstrates the challenge within this approach to retrieve usable PS over the marshy and moist natural surfaces of the island.

Displacement for selected points

Figure 11 shows time-series of displacement between 09/2018 and 09/2019 (period asc3) for selected areas on Bhasan Char as indicated in Figures 9 and 10. The displayed values represent the average displacement of all PS within a radius of 100 m within these areas. To statistically support the trends indicated by the regression lines, the coefficients of determination (R2) and the p-value (indicating the level of significance) were calculated.

As already indicated in the previous section, the built-up area (A) shows a quite stable temporal development throughout all 251 points with displacement values ranging within −2 and +2 mm, except for one outlier in the last quarter of the period. As this outlier strongly affects the fitting of the overall trend line (plotted in red), the slight ascending gradient is just a matter of computation and does not mean a general uplift of this area. This is supported by the near zero R2 of the line and its high probability value (p = 0.304) which both confirm that the observed trend is rather insignificant.

A stronger subsidence of over 20 mm in total is shown at the western embankment (B) and the southern part of the island (D). Both have a clear descending trend with R2 values larger 0.3 and probability values

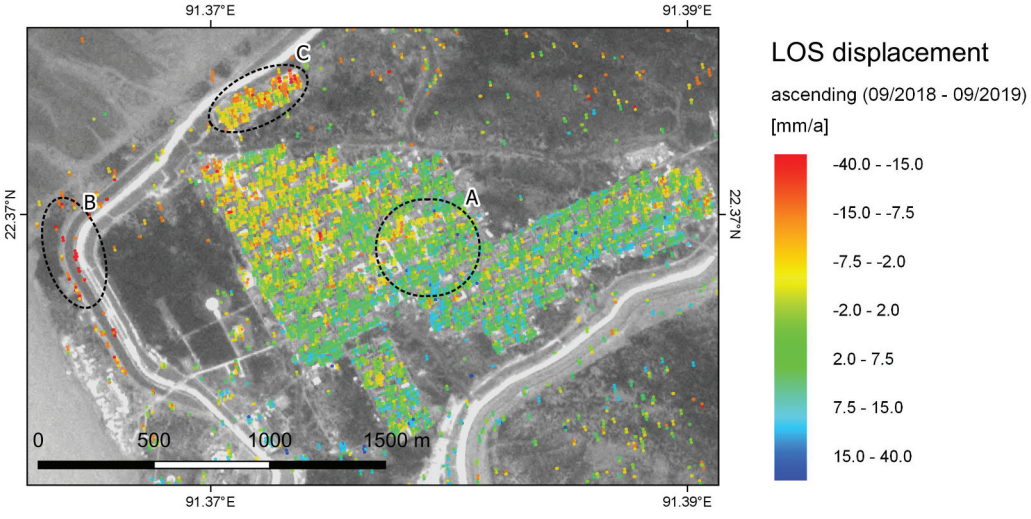

Figure 10. Detailed map of LOS displacement between 09/2018 and 09/2019 for the built-up area on Bhasan Char.

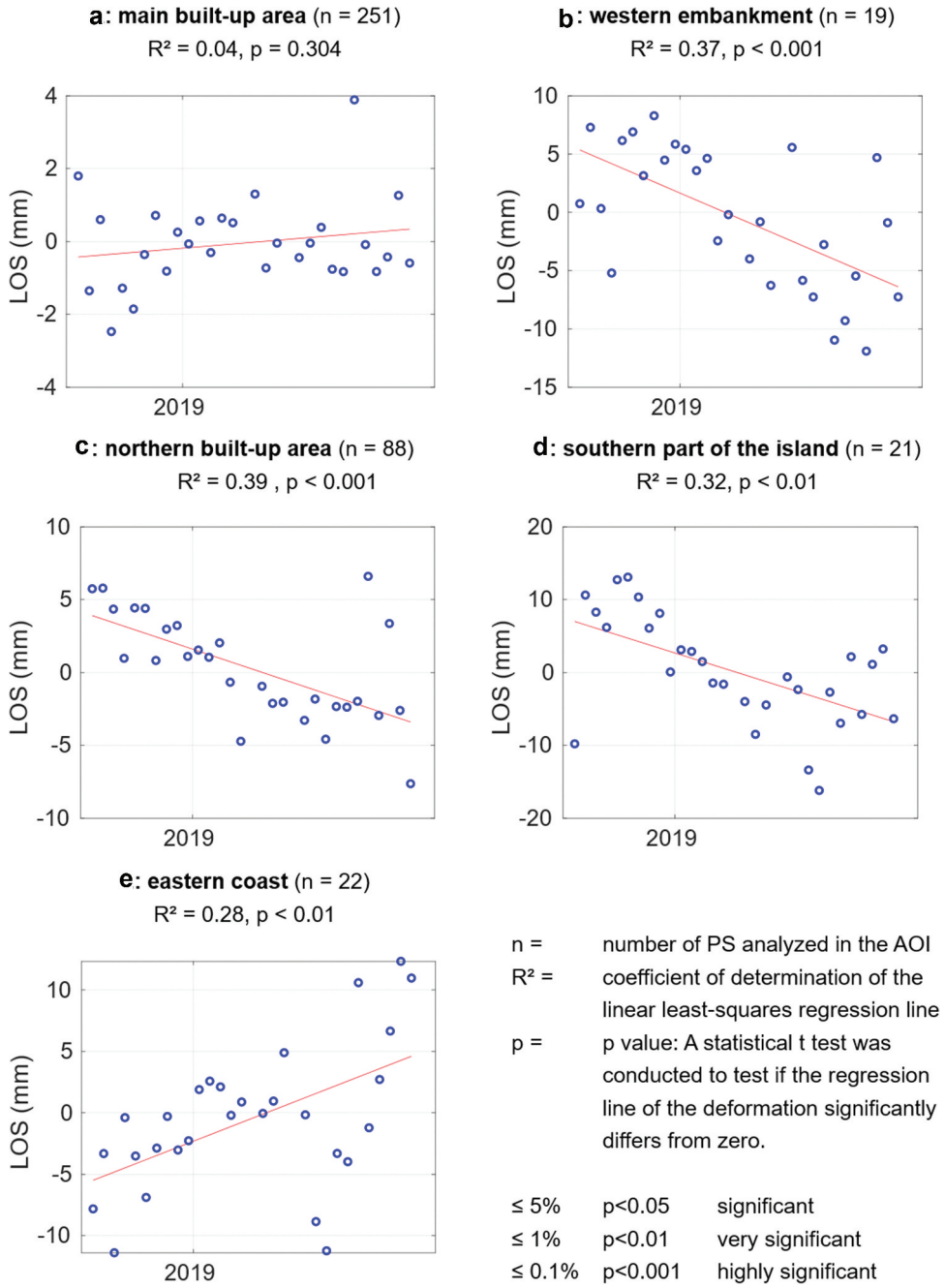

Figure 11. Time-series of displacement between 09/2018 and 09/2019 for selected areas on Bhasan Char (as shown in Figures 8 and 9). The numbers in brackets indicate the number of PS within a radius of 100 meters.

<0.01 and <0.001 respectivel0.001, respectively, which indicate that these trends are not caused by chance. The larger variation in B can have several reasons: Most likely, because it was based on a considerably smaller number of PS within the radius of 100 m (n = 19). In contrast, the average displacement of D was calculated based on a denser pattern of PS (n = 88), thus leading to a clearer downward trend with less temporal variation. Another important aspect is that the different areas on the island can generally underlie non-linear deformation trends which are naturally characterized by large variations along the regression line. This, and the fact that each point in the regression is an aggregation of 19 to 251 proximate PS, limits the overall conclusions to be drawn from the temporal plots.

While the larger built-up area shows a temporal stability, the smaller dispatched buildings north of it (C) indicate a downward trend with a coefficient of determination of R2 = 0.28 and p < 0.01. It shows the same outliers than in the main built-up area which could be explained by heavy rains, as the rainy season is from June to August with monthly precipitations above 800 mm. Such heavy rains are reported to cause atmospheric path delays in the phase signal and can have a large impact on the resulting phase information (Ding et al., 2008). Yet, the closeness of the smaller built-up area to the coast might indicate that it does

stand on successively compacting ground. We tested the differences of deformation rates between the regions for significance in section 3.4.

A clear uplift is shown for the area along the eastern coast (E) with a total range of over 20 mm per year. As this area is over 5 km away from the built-up areas, it is unlikely that it is caused by human activity or anthropogenic impact, but rather a matter of natural surface dynamics. Again, such extreme values over the time of only one year indicate that the island is not stable in general.

Statistical evaluation

To further analyse the results of this study, a one-way analysis of variance (ANOVA, Fisher, 1954) was conducted to test for significant differences regarding surface velocities between the detail regions highlighted in Figure 11 and also between the three investigated periods (asc1, asc2, asc3). This gives further insights on the trends and relations which were discussed in the previous section. Figure 12 shows box plots of the surface velocities for the detail regions (left) and the three analysed periods (right). It visually underlines that region A (within newly built-up area) has little variance compared to the other regions and only small overall deformation rates but has a higher number of statistical outliers which cause the slightly positive mean. It also confirms the clear uplift trend of the eastern coast (region E), compared to the subsiding southern and north-western coast areas (B, C and D). However, these five regions contain a considerably different number of PS which can potentially affect the homogeneity of variances which is a basic requirement of an ANOVA (Keppel & Wickens, 2004). And also, the number of PS differs between the three investigated periods (Table 1). We therefore conducted Bartlett's test to confirm variance homogeneity ($p < 0.001$) for both cases. A post-hoc analysis (Tukey, 1949) was computed to test for pairwise significant differences. Table 2 shows the adjusted p-values between all five regions. Except for B and D ($p = 0.9$), the null hypothesis (H0) is rejected, which means that displacement values between these pairs differ with very high significance ($p < 0.001$). These calculations show that most of the detail regions visualized in Figure 9 have distinct spatial patterns which are statistically significant. To confirm the stability of different parts of the island, this statistical evaluation should be maintained or even extended in further studies. The second boxplot (Figure 12, right) shows the similarity of all three investigated periods. The continuous decrease of both the degree of dispersion and the interquartile range might be interpreted as signs of stabilization of the island over time, but these differences are of subtle nature and cannot serve as a clear evidence. This is underlined by the Tukey test of the three periods which clearly reports mean differences below −0.015 mm/a and, more importantly, adjusted p-values of 0.9 (Table 3). Accordingly, the null hypothesis cannot be rejected, which means that there is no significant difference in deformation between the three investigated periods. In the consequence, this also means that there is no statistical evidence for human impact on the deformation of the island.

Discussion

The results presented in the previous section demonstrate that persistent scatterer interferometry can be applied to measure elevation dynamics of islands, even if their moist surfaces with widely absent artificial structures are a challenge. The findings indicate that the island is characterized by active compaction processes and heterogeneous surface displacement patterns; however, the data does not attest the construction activities as the main reason. Furthermore, there are several points to discuss.

The different densities of usable PS (Table 1) can partly be explained by the lack of human activity during asc1 and the presence of solid buildings in asc3. However, the initial number of PS candidates already significantly differs for the four periods. Despite that, all

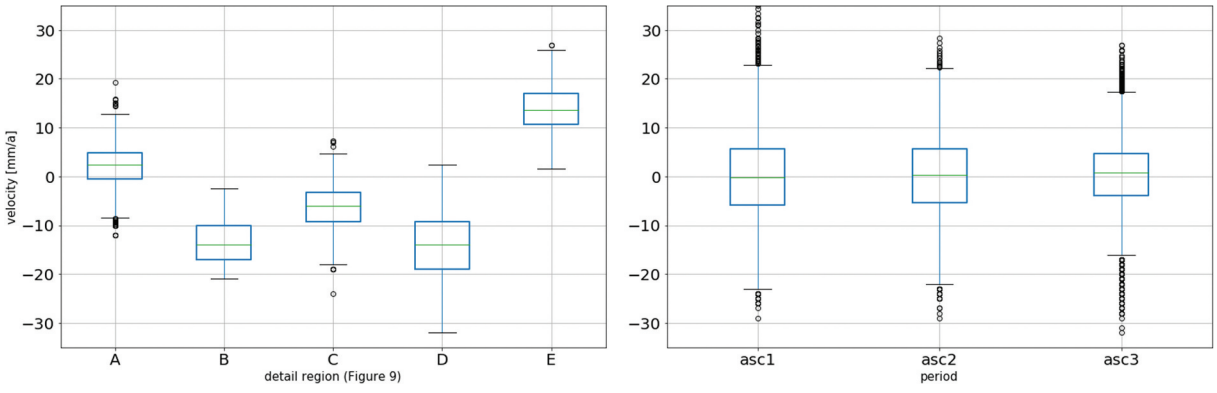

Figure 12. Box plots of the velocity [mm/a] for the three detail regions (left) and the three analyzed periods (right).

Table 2. Pairwise test for significant deformation differences between the five detail regions (A-E).

region 1	region 2	mean difference	adjusted p	5%	95%	reject H0
A	B	−15.7	0.001	−17.8	−13.6	true
A	C	−8.4	0.001	−9.1	−7.6	true
A	D	−16.1	0.001	−16.9	−15.4	true
A	E	12.0	0.001	10.4	13.7	true
B	C	7.3	0.001	5.2	9.5	true
B	D	−0.4	0.9	−2.5	1.7	false
B	E	27.7	0.001	25.2	30.3	true
C	D	−7.8	0.001	−8.7	−6.8	true
C	E	20.4	0.001	18.7	22.1	true
D	E	28.2	0.001	26.4	29.9	true

Table 3. Pairwise test for significant deformation differences between the three analysed periods.

period 1	period 2	mean difference	adjusted p	5%	95%	reject H0
asc1	asc2	−0.00370	0.9	−0.286	0.279	false
asc1	asc3	−0.01430	0.9	−0.268	0.239	false
asc2	asc3	−0.01060	0.9	−0.240	0.219	false

of the periods have the duration of 1 year and consist of 26 to 31 images, the amount of PS candidates of period dsc (n = 172,153) clearly stands out. This can be explained by a slightly different coverage of the descending track and the larger proportion of land pixels. However, after applying the processing chain as described in section 2.4 and after spatial normalization, the descending period reveals an even lower density (79 PS/km^2) than the other three.

Generally, one of the main challenges was to retrieve a sufficient density of usable PS while at the same time excluding pixels with low quality or noise. The high water content of the island's surface and the strong seasonal variability with monsoonal rains occurring in every investigated period prevented the identification of suitable PS that are evenly distributed in both the spatial and temporal domain. This was handled by increasing the amplitude dispersion threshold to 0.42 in the beginning and by raising the maximum allowed noisy pixels to 25 per square kilometre. However, this inevitably led to the presence of PS with inaccurate or even wrong phase information. This can be dangerous for the construction of the PS network and the later unwrapping because it leads to the wrong estimation of surface velocities (A. Hooper et al., 2012). The spatial patterns shown in Figures 9 and 10 do not indicate larger unwrapping errors. It would be good in terms of validation to put these findings into a context, for example, GPS measurements of surface heights, as proposed by Wei et al. (2010). However, due to the sensitive nature of the case, it is unlikely that measurements about this island will be made publicly available. As an alternative, the correlation of temporal surface patterns with sea level variations in the Bay of Bengal, which could be measured by tide gauges or satellite altimetry (Ghosh et al., 2018), could bring additional insights and help to explain to what extent the observed changes are triggered by tidal dynamics.

One option for future studies would be to exclude single images which are acquired during the monsoon season and visibly cause faulty outliers, as demonstrated by the time-series graphs in Figure 11, and recompute the period without their contributions. However, this only works when a small fraction of products is affected. Removing entire months of rainy seasons is surely counterproductive to the PSI principle. Accordingly, higher levels of atmospheric correction should be taken into consideration in monsoonal environments (compared to the temporal low-pass filter applied in this study). For example, packages such as the Toolbox for Reducing Atmospheric InSAR Noise (TRAIN, Bekaert et al., 2015) or the Generic Atmospheric Correction Online Service for InSAR (GACOS, Yu et al., 2018) allow to estimate the variations in atmospheric phase screen under conditions of non-linear deformation as well, as it might be the case for Bhasan Char. As this study is considered a first proof of concept, these options should be considered for future research.

Another way to retrieve more stable time-series graphs is the observation of longer time spans. However, as it turned out in this study, periods longer than one year lead to a drastic reduction of usable PS due to increasing temporal decorrelation. This again underlies the trade-off between acquiring a sufficient density of points and maintaining a low level of noisy pixels which had to be accomplished in this case.

A more promising technique could solve most of the problems discussed above: Instead of pairing one master image with all other images (slaves) within an investigated period, the so-called Small BAselineSubset (SBAS) approach suggests the computation of interferograms between all possible image pairs within a defined temporal and perpendicular baseline (Berardino et al., 2002). This has several advantages: The time between two images forming an interferogram can be considerably reduced, thus leading to less temporal decorrelation and a more stable phase information. Furthermore, the construction of a network of analysed dates leads to multiple combinations of image pairs which significantly increases the number of retrievable displacements within the investigated period. Lastly, the reduction of temporal decorrelation allows to observe longer-time-series and therefore replaces the necessity to split the investigated period into three individual periods of one-year length with possibly different processing parameters (Table 1), as it was done in this study. Figure 13 shows the baseline chart if all image pairs with a perpendicular baseline of smaller than 120 m and a temporal baseline of maximal were included in the analysis. This would allow to compute 491 interferograms over the investigated period. Of course, this strongly increases the stability of the analysed phase information, leads to a higher density of

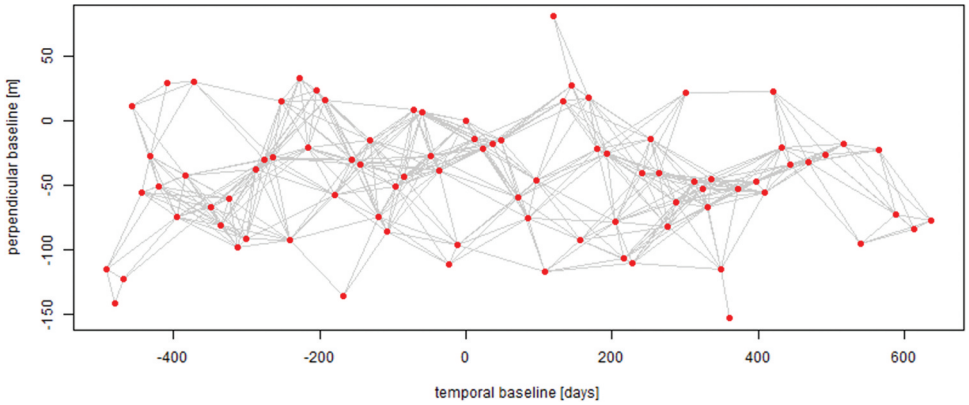

Figure 13. Baseline chart for the entire investigated period (08/2016-09/2019) allowing perpendicular baselines of 120 metres and temporal baselines of 65 days at maximum.

usable points, and a notably lower proportion of noisy pixels. From a computational perspective, however, this also leads to a considerable increase of processing time and storage demand. Furthermore, the preparation interferogram products for the SBAS approach is currently not yet supported in the SNAP software which was used in this study. Yet, to achieve more reliable results with a higher spatial density of PS, future studies of Bhasan Char shout make use of the SBAS approach or consider incorporating distributed scatterers (DS) which are defined as pixels whose neighbouring pixels share similar statistical behaviour (Shamshiri et al., 2018).

Conclusions and outlook

This study showed how C-band radar satellite information can be used to characterize the dynamics of the island of Bhasan Char in the Bay of Bengal. It was conducted in anticipation of the planned relocation of about 100,000 refugees which are currently hosted in Bangladesh. It is an initial proof of concept demonstrating that multi-temporal persistent scatterer interferometry (PSI) can help to identify surface deformations between 2016 and 2019. Our study gives first indications that the island already showed surface variations before the construction works began in 2018. The statistical comparison of the three investigated periods could not confirm the indication that some of the construction caused additional subsidence of the island, for instance, because of soil compaction. The statistical evaluations in this study proved that the observed trends for most selected areas (Figure 11) are significant and cannot yet give final evidence for the instability of the island without external validation data. Furthermore, the investigated period is too short to reliably detect long-term trends superimposing the continuous dynamics demonstrated by the PSI analysis. Neither can a linear trend of compaction be assumed nor a digressive trend of settling compaction due to the marine influences the island is exposed to. For the future assessment of risks, the deformation regime of the island (e.g., linear, seasonal, or settling; Larsen et al., 2020) should be assessed, as well as the role of sea level rise. Additionally, the temporal behaviour of soil compaction as a result of both natural impacts and higher construction volume loads should be further monitored.

Despite the lack of in-situ measurements on surface changes as a validation, the main challenges emanate from the surface of the island which largely consists of moist sands and only few stable radar targets. This resulted in the need to loosen the criteria for the selection of suitable persistent scatterers (PS), potentially introducing errors in the analysed data. Future studies must be carried out on this topic, ideally based on the SBAS approach, to increase the amount of computed interferograms and to observe the entire period covered by Sentinel-1 data.

Yet, this study shall partly respond to the call of Ullah (2011) who claimed that Rohingyas and their protection were given too little research attention throughout their eventful history. Because, regardless of the trigger of the observed dynamics, their implications for the safety of the people to be relocated on this island are still valid: Not only are their sinking coastlines prone to lateral erosion (Islam et al., 2019), but also does the sandbank's subsidence combined with its the very low altitude of 2.84 m lead to an increased vulnerability to flooding with respect to sea-level variations (Banerjee, 2020). Strong seasonality furthermore increases the stress on islands in this area, because they are threatened by droughts during the summer months and by erosion through flash floods from the mainland which are surging into the bay areas during the monsoon period (Bandyopadhyay et al., 2014).

We therefore encourage the scientific community to engage in investigations of this vulnerable area and share their results to assess the potential risk of the Rohingya people in need. Our work is predominantly based on open data and open source software and

wants to promote the open science initiative by sharing experiences about obstacles and opportunities of geospatial analyses to tackle current challenges of global change.

Acknowledgments

Sentinel-1 data was provided by the European Space Agency (ESA) within the Copernicus programme. The authors thank Edward Cahill for the language editing of this manuscript and Luisa Minich for revising the figures.

Disclosure statement

No potential conflict of interest was reported by the authors.

ORCID

Andreas Braun http://orcid.org/0000-0001-8630-1389
Thorsten Höser http://orcid.org/0000-0002-7179-3664
José Manuel Delgado Blasco http://orcid.org/0000-0003-0098-3046

References

Abidin, H., Andreas, H., Gumilar, I., Sidiq, T. P., & Fukuda, Y. (2013). 'Land subsidence in coastal city of Semarang (Indonesia): Characteristics, impacts and causes'. *Geomatics, Natural Hazards and Risk*, *4*(3), 226–240. https://doi.org/10.1080/19475705.2012.692336

Aly, M. H., Klein, A. G., Zebker, H. A., & Giardino, J. R. (2012). 'Land subsidence in the Nile Delta of Egypt observed by persistent scatterer interferometry'. *Remote Sensing Letters*, *3*(7), 621–630. https://doi.org/10.1080/01431161.2011.652311

Amitrano, D., Di Martino, G., Iodice, A., Riccio, D., Ruello, G., Papa, M. N., Ciervo, F., & Koussoube, Y. (2013) Synthetic Aperture Radars for humanitarian purposes: Products and opportunities, *IEEE Global Humanitarian Technology Conference*. Trivandrum, India, 23–24 August 2013, IEEE, 457–462.

Anderson, D., & Lochery, E. (2008). Violence and exodus in Kenya's Rift Valley, 2008: Predictable and preventable? *Journal of Eastern African Studies*, *2*(2), 328–343. https://doi.org/10.1080/17531050802095536

Bandyopadhyay, S., Kar, N. S., Das, S., & Sen, J. (2014). River systems and water resources of West Bengal: A review. *Geological Society of India Special Publication*, *3*, 63–84. http://doi.org/10.17491/cgsi/2014/62893

Banerjee, S. (2020) *From Cox's Bazar to Bhasan Char: An assessment of Bangladesh's relocation plan for Rohingya refugees [Online]*, Observer Research Foundation (ORF issue brief 357). Retrieved May 10, 2020, from. https://www.orfonline.org/research/from-coxs-bazar-to-bhasan-char-an-assessment-of-bangladeshs-relocation-plan-for-rohingya-refugees-65784

Bashar, I. (2017). Exploitation of the Rohingya crisis by jihadist groups: Implications for Bangladesh's internal security. *Counter Terrorist Trends and Analyses*, *9*(9), 5–7. https://www.jstor.org/stable/26351550

Bekaert, D. P. S., Walters, R. J., Wright, T. J., Hooper, A., & Parker, D. J. (2015). Statistical comparison of InSAR tropospheric correction techniques. *Remote Sensing of Environment*, *170*, 40–47. https://doi.org/10.1016/j.rse.2015.08.035

Berardino, P., Fornaro, G., Lanari, R., & Sansosti, E. (2002). A new algorithm for surface deformation monitoring based on small baseline differential SAR interferograms. *IEEE Transactions on Geoscience and Remote Sensing*, *40*(11), 2375–2383. https://doi.org/10.1109/TGRS.2002.803792

Bjorgo, E. (2000). Using very high spatial resolution multispectral satellite sensor imagery to monitor refugee camps. *International Journal of Remote Sensing*, *21*(3), 611–616. https://doi.org/10.1080/014311600210786

Braun, A. (2018). Assessment of building damage in Raqqa during the Syrian civil war using time-series of radar satellite imagery. *Geographic Information Science*, *1*, 228–242. https://doi.org/10.1553/giscience2018_01_s228

Braun, A., Fakhri, F., & Hochschild, V. (2019). Refugee camp monitoring and environmental change assessment of Kutupalong, Bangladesh, based on radar imagery of Sentinel-1 and Alos-2. *Remote Sensing*, *11*(17), 2047. https://doi.org/10.3390/rs11172047

Braun, A., & Hochschild, V. (2018) *Mapping sea surface dynamics in the context of displaced persons - the case of rohingya refugees in bangladesh* [Online], Frascati, Italy. Retrieved October 15, 2019, from. http://mwbs2018.esa.int/files/presentation159.pdf

Chen, C. W., & Zebker, H. A. (2001). Two-dimensional phase unwrapping with use of statistical models for cost functions in nonlinear optimization. *Journal of the Optical Society of America. A, Optics, Image Science, and Vision*, *18*(2), 338–351. https://doi.org/10.1364/JOSAA.18.000338

Cian, F., Delgado Blasco, J. M., & Carrera, L. (2019). 'Sentinel-1 for monitoring land subsidence of coastal cities in Africa using PS InSAR: A methodology based on the integration of SNAP and StaMPS'. *Geosciences*, *9*(3), p. 124. https://doi.org/10.3390/geosciences9030124

Colesanti, C., Ferretti, A., Prati, C., & Rocca, F. (2003). 'Monitoring landslides and tectonic motions with the Permanent Scatterers Technique'. *Engineering Geology*, *68*(1–2), 3–14. https://doi.org/10.1016/S0013-7952(02)00195-3

Crosetto, M., Monserrat, O., Cuevas-González, M., Devanthéry, N., & Crippa, B. (2016). Persistent Scatterer Interferometry: A review. *ISPRS Journal of Photogrammetry and Remote Sensing*, *115*, 78–89. https://doi.org/10.1016/j.isprsjprs.2015.10.011.

Crosetto, M., Monserrat, O., Devanthéry, N., Cuevas-González, M., Barra, A., & Crippa, B. (2016) 'Persistent scatterer interferometry using Sentinel-1 data', *Proceedings of the International Archives of the Photogrammetry, Remote Sensing and Spatial Information Sciences Congress*, 12–19 July. Prague, Czech Republic, 835–839.

d'Oleire-Oltmanns, S., Tiede, D., Krauß, T. and Wendt, L. (2018) Object-based 3D damage assessment using surface models derived from mixed-date stereo models, *From pixels to ecosystems and global sustainability*. Montpellier, France, 18–22 June 2018. GEOBIA'2018, 1–12.

Da Lio, C., & Tosi, L. (2018). 'Land subsidence in the Friuli Venezia Giulia coastal plain, Italy: 1992-2010 results from SAR-based interferometry'. *The Science of the Total Environment*, *633*, 752–764. https://doi.org/10.1016/j.scitotenv.2018.03.244

Dehghani, M., Zoej, M. J. V., Hooper, A., Hanssen, R. F., Entezam, I., & Saatchi, S. (2013). 'Natural versus

anthropogenic subsidence of Venice'. *Scientific Reports*, *3* (2710), 1–9. https://doi.org/10.1038/srep02710

Delgado Blasco, J. M. (2019) *snap2stamps: GitHub repository [Online]*. Retrieved October 15, 2019, from, https://github.com/mdelgadoblasco/snap2stamps

Delgado Blasco, J. M., & Foumelis, M. (2018) *snap2stamps: Automated SNAP Sentinel-1 DInSAR processing for StaMPS PSI with open source tools [Online]*. Zenado. Retrieved October 15, 2019, from. https://zenodo.org/record/1322353

Delgado Blasco, J. M., Foumelis, M., Stewart, C., & Hooper, A. (2019). 'Measuring urban subsidence in the Rome metropolitan area (Italy) with Sentinel-1 SNAP-StaMPS persistent scatterer interferometry'. *Remote Sensing*, *11*(2), 129. https://doi.org/10.3390/rs11020129

Ding, X.-L., Li, Z.-W., Zhu, -J.-J., Feng, G.-C., & Long, J.-P. (2008). 'Atmospheric effects on InSAR measurements and their mitigation'. *Sensors*, *8*(9), 5426–5448. https://doi.org/10.3390/s8095426

Ferretti, A., Monti-Guarnieri, A., Prati, C., Rocca, F., & Massonnet, D. (2007). *InSAR principles. Guidelines for SAR interferometry processing and interpretation*. Frascati, Italy: European Space Agency.

Ferretti, A., Prati, C., & Rocca, F. (2000). 'Nonlinear subsidence rate estimation using permanent scatterers in differential SAR interferometry'. *IEEE Transactions on Geoscience and Remote Sensing*, *38*(5), 2202–2212. https://doi.org/10.1109/36.868878

Ferretti, A., Prati, C., & Rocca, F. (2001). 'Permanent scatterers in SAR interferometry'. *IEEE Transactions on Geoscience and Remote Sensing*, *39*(1), 8–20. https://doi.org/10.1109/36.898661

Fisher, R. (1954). 'The analysis of variance with various binomial transformations'. *Biometrics*, *10*(1), 130–139. https://doi.org/10.2307/3001667

Foumelis, M., Delgado Blasco, J. M., Desnos, Y.-L., Engdahl, M., Fernandez, D., Veci, L., Lu, J., & Wong, C. (2018) 'ESA SNAP-StaMPS integrated processing for Sentinel-1 persistent scatterer interferometry', *IEEE International Geoscience and Remote Sensing Symposium*. Valencia, Spain, 22–27 July 2018, IEEE, 1364–1367.

Ghorbanzadeh, O., Tiede, D., Dabiri, Z., Sudmanns, M., & Lang, S. (2018). Dwelling extraction in refugee camps using CNN: First experiences and lessons learnt. *International Archives of the Photogrammetry, Remote Sensing & Spatial Information Sciences*. https://doi.org/10.5194/isprs-archives-XLII-1-161–2018

Ghosh, S., Hazra, S., Nandy, S., Mondal, P. P., Watham, T., & Kushwaha, S. P. S. (2018). 'Trends of sea level in the Bay of Bengal using altimetry and other complementary techniques'. *Journal of Spatial Science*, *63*(1), 49–62. https://doi.org/10.1080/14498596.2017.1348309

Giada, S., Groeve, T. D., Ehrlich, D., & Soille, P. (2003). 'Information extraction from very high resolution satellite imagery over Lukole refugee camp, Tanzania'. *International Journal of Remote Sensing*, *24*(22), 4251–4266. https://doi.org/10.1080/0143116021000035021

Grandin, R. (2015) 'Interferometric processing of SLC Sentinel-1 TOPS data', *Advances in the science and applications of SAR Interferometry and Sentinel-1*. Frascati, Italy, 23-27 March 2015, 1–8.

Guhathakurta, M. (2017). 'Understanding violence, strategising protection: Perspectives from Rohingya refugees in Bangladesh'. *Asian Journal of Social Science*, *45*(6), 639–665. https://doi.org/10.1163/15685314-04506003

Hagenlocher, M., Lang, S., & Tiede, D. (2012). 'Integrated assessment of the environmental impact of an IDP camp in Sudan based on very high resolution multi-temporal satellite imagery'. *Remote Sensing of Environment*, *126*, 27–38. https://doi.org/10.1016/j.rse.2012.08.010

Hanssen, R. F. (2001). *Radar interferometry. Data interpretation and error analysis*. Springer.

Hooper, A. (2018). *StaMPS Persistent Scatterer Practical: ESA Land Training Course, Leicester, 10-14th September 2018 [Online]*. University of Leicester. Retrieved May 10, 2020, from http://eoscience.esa.int/landtraining2018/files/materials/D3B2_Stamps_S1_PS_Exercise_2018.pdf

Hooper, A., Bekaert, D., Ekbal, H., & Spaans, K. (2018). *StaMPS/MTI manual: Version 4.1b [Online]*. School of Earth and Environment, University of Leeds. Retrieved October 15, 2019, from https://github.com/dbekaert/StaMPS/blob/master/Manual/StaMPS_Manual.pdf

Hooper, A., Bekaert, D., Spaans, K., & Arıkan, M. (2012). 'Recent advances in SAR interferometry time series analysis for measuring crustal deformation'. *Tectonophysics*, *514-517*, 1–13. https://doi.org/10.1016/j.tecto.2011.10.013

Hooper, A., Segall, P., & Zebker, H. (2007). 'Persistent scatterer interferometric synthetic aperture radar for crustal deformation analysis, with application to Volcán Alcedo, Galápagos'. *Journal of Geophysical Research*, *112* (B7), 1–21. https://doi.org/10.1029/2006JB004763

Hu, B., Chen, J., & Zhang, X. (2019). 'Monitoring the land subsidence area in a coastal urban area with InSAR and GNSS'. *Sensors*, *19*(14), p. 3181. https://doi.org/10.3390/s19143181

Islam, M. S., Rahman, M. A., Chowdhury, T. A., Begum, A., Shahid, T., & Islam, M. A. (2019) 'Geomorphologic change of Bhasan Char island. The new home of Rohingya refugees in the Bay of Bengal', *Rohingya-2019*. Dhaka, Bangladesh, 28–29 July.

Keppel, G., & Wickens, T. D. (2004). *Design and analysis: A researcher's handbook*. N.J, Pearson Prentice Hall.

Kim, J. S., Kim, D. J., Kim, S.-W., Won, J. S., & Moon, W. M. (2007). 'Monitoring of urban land surface subsidence using PSInSAR'. *International Journal of Applied Earth Observation and Geoinformation*, *11*, 59–73. https://doi.org/10.1007/BF02910381

Kim, S.-W., Wdowinski, S., Dixon, T. H., Amelung, F., Kim, J. W., & Won, J.-S. (2010). 'Measurements and predictions of subsidence induced by soil consolidation using persistent scatterer InSAR and a hyperbolic model'. *Geophysical Research Letters*, *37*(5), 1–5. https://doi.org/10.1029/2009GL041644

Knoth, C., & Pebesma, E. (2017). 'Detecting dwelling destruction in Darfur through object-based change analysis of very high-resolution imagery'. *International Journal of Remote Sensing*, *38*(1), 273–295. https://doi.org/10.1080/01431161.2016.1266105

Kolla, V., Moore, D. G., & Curray, J. R. (1976). 'Recent bottom-current activity in the deep western Bay of Bengal'. *Marine Geology*, *21*(4), 255–270. https://doi.org/10.1016/0025-3227(76)90010-4

Laneve, G., Santilli, G., & Lingenfelder, I. (2006) Development of automatic techniques for refugee camps monitoring using very high spatial resolution (VHSR) satellite imagery, *2006 IEEE International Symposium on Geoscience and Remote Sensing*. Denver, Colorado, 31 July - 4 August 2006, IEEE, 841–845.

Lang, S., Füreder, P., Kranz, O., Card, B., Roberts, S., & Papp, A. (2015). 'Humanitarian emergencies: Causes, traits and impacts as observed by remote sensing'. In P. S. Thenkabail (Ed.), *Remote sensing of water resources, disasters, and urban studies* (pp. 483–512). CRC Press.

Lang, S., Füreder, P., Riedler, B., Wendt, L., Braun, A., Tiede, D., Schöpfer, E., Zeil, P., Spröhnle, K., Kulessa, K., Rogenhofer, E., Bäuerl, M., Öze, A., Schwendemann, G., & Hochschild, V. (2019). 'Earth observation tools and services to increase the effectiveness of humanitarian assistance'. *Europen Journal of Remote Sensing*, 1–19. https://doi.org/10.1080/22797254.2019.1684208

Lang, S., Tiede, D., Hölbling, D., Füreder, P., & Zeil, P. (2010). 'Earth observation (EO)-based ex post assessment of internally displaced person (IDP) camp evolution and population dynamics in Zam Zam, Darfur'. *International Journal of Remote Sensing*, *31*(21), 5709–5731. https://doi.org/10.1080/01431161.2010.496803

Larsen, Y., Markinovic, P., Dehls, J. F., Bredal, M., Bishop, C., Jøkulsson, G., Frauenfelder, R., Salazar, S. E., Vöge, M., Constantini, M., Minati, F., Trillo, F., Ferretti, A., Capes, R., Bianchi, M., Parizzi, A., Brcic, R., Casu, F., Lanari, R., Manunta, M., … Zinno, I. (2020) *Copernicus Land Monitoring Service: European Ground Motion Service: Service Implementation Plan and Product Specification Report (Version 1.01) [Online]*. https://land.copernicus.eu/user-corner/technical-library/egms-specification-and-implementation-plan.

Li, X., & Li, D. (2014). 'Can night-time light images play a role in evaluating the Syrian Crisis?'. *International Journal of Remote Sensing*, *35*(18), 6648–6661. https://doi.org/10.1080/01431161.2014.971469

Lodhi, M. A., Echavarria, F. R., & Keithley, C. (1998). 'Using remote sensing data to monitor land cover changes near Afghan refugee camps in northern Pakistan'. *Geocarto International*, *13*(1), 33–39. https://doi.org/10.1080/10106049809354626

Martin, M. F., Margesson, R., & Vaughn, B. (2018). The Rohingya crises in Bangladesh and Burma. *Current Politics and Economics of South, Southeastern, and Central Asia*, *27*(3/4), 333–375. https://fas.org/sgp/crs/row/R45016.pdf

Marx, A., & Goward, S. (2013). 'Remote sensing in human rights and international humanitarian law monitoring: Concepts and methods'. *Geographical Review*, *103*(1), 100–111. https://doi.org/10.1111/j.1931-0846.2013.00188.x

Milton, A. H., Rahman, M. A., Hussain, S., Jindal, C., Choudhury, S., Akter, S., Ferdousi, S., Mouly, T. A., Hall, J., & Efird, J. T. (2017). 'Trapped in statelessness: Rohingya refugees in Bangladesh'. *International Journal of Environmental Research and Public Health*, *14*(8), 942. https://doi.org/10.3390/ijerph14080942

Nasrin, T. (2019). 'Energy estimations and hypothetical design of an exclusive tourism spot in coastal region named "Bhasan Char" of Bangladesh'. *Journal of Power Electronics & Power Systems*, *9*(3), 1–9. https://doi.org/10.37591/.v9i3.2775

O'Connell, T., & Young, S. (2014). 'No more hidden secrets: Human rights violation and remote sensing'. *Genocide Studies and Prevention*, *8*(3), 5–31. https://doi.org/10.5038/1911-9933.8.3.3

Osmanoğlu, B., Dixon, T. H., Wdowinski, S., Cabral-Cano, E., & Jiang, Y. (2011). Mexico City subsidence observed with persistent scatterer InSAR. *International Journal of Applied Earth Observation and Geoinformation*, *13*(1), 1–12. https://doi.org/10.1016/j.jag.2010.05.009.

PDGS (2020) *POD Precise Orbit Ephemerides [AUX_POEORB]: European Space Agency [Online]*, Payload Data Ground Segment. Retrieved October, 15 2019, from. https://qc.sentinel1.eo.esa.int/

Quinn, J. A., Nyhan, M. M., Navarro, C., Coluccia, D., Bromley, L., & Luengo-Oroz, M. (2018). 'Humanitarian applications of machine learning with remote-sensing data: Review and case study in refugee settlement mapping'. *Philosophical Transactions of the Royal Society A: Mathematical, Physical and Engineering Sciences*, *376*(2128), 20170363. https://doi.org/10.1098/rsta.2017.0363

Rahman, U. (2010). 'The Rohingya refugee: A security dilemma for Bangladesh'. *Journal of Immigrant & Refugee Studies*, *8*(2), 233–239. https://doi.org/10.1080/15562941003792135

Reynaud, J.-Y., & Dalrymple, R. W. (2012). 'Shallow-Marine Tidal Deposits'. In R.A. Davis & R.W. Dalrymple (Eds.), *Principles of Tidal Sedimentology* (pp. 335–369). Dordrecht.

Schaefer, L. N., Di Traglia, F., Chaussard, E., Lu, Z., Nolesini, T., & Casagli, N. (2019). 'Monitoring volcano slope instability with Synthetic Aperture Radar: A review and new data from Pacaya (Guatemala) and Stromboli (Italy) volcanoes'. *Earth-Science Reviews*, *192*, 236–257. https://doi.org/10.1016/j.earscirev.2019.03.009

Seidel, M., Marzahn, P., & Ludwig, R. (2016). Dyke MonitoringMonitorin by the Means of Persistent Scattering Interferometry at the Coast of Northern Germany. *ISPRS - International Archives of the Photogrammetry, Remote Sensing and Spatial Information Sciences*, *XLI-B*(8), 169–173. https://doi.org/10.5194/isprsarchives-XLI-B8-169-2016

Shamshiri, R., Nahavandchi, H., Motagh, M., & Hooper, A. (2018). 'Efficient Ground Surface Displacement Monitoring Using Sentinel-1 Data: Integrating Distributed Scatterers (DS) Identified Using Two-Sample t-Test with Persistent Scatterers (PS)'. *Remote Sensing*, *10*(5), p. 794. https://doi.org/10.3390/rs10050794

Solari, L., Ciampalini, A., Raspini, F., Bianchini, S., & Moretti, S. (2016). 'PSInSAR analysis in the Pisa urban area (Italy): A case study of subsidence related to stratigraphical factors and urbanization'. *Remote Sensing*, *8*(2), 120. https://doi.org/10.3390/rs8020120.

Spröhnle, K., Fuchs, E.-M., & Pelizari, P. A. (2017). 'Object-based analysis and fusion of optical and SAR satellite data for dwelling detection in refugee camps'. *IEEE Journal of Selected Topics in Applied Earth Observations and Remote Sensing*, *10*(5), 1780–1791. https://doi.org/10.1109/JSTARS.2017.2664982

Sulik, J. J., & Edwards, S. (2010). 'Feature extraction for Darfur: Geospatial applications in the documentation of human rights abuses'. *International Journal of Remote Sensing*, *31*(10), 2521–2533. https://doi.org/10.1080/01431161003698369

Sunny, M. J., Rahman, M. A., & Matin, M. A. (2019) 'Affordable electricity for Bhashan Char from renewable energy', *2019 International Conference on Electrical, Computer and Communication Engineering (ECCE)*. Cox'sBazar, Bangladesh, 07–09 February 2019, IEEE, 1–5.

Talwani, M., Desa, M. A., Ismaiel, M., & Sree Krishna, K. (2016). 'The Tectonic origin of the Bay of Bengal and Bangladesh'. *Journal of Geophysical Research: Solid Earth*, *121*(7), 4836–4851. https://doi.org/10.1002/2015JB012734

Teatini, P., Tosi, L., Strozzi, T., Carbognin, L., Cecconi, G., Rosselli, R., & Libardo, S. (2012). Resolving land subsidence within the Venice Lagoon by persistent scatterer SAR interferometry. *Physics and Chemistry of the Earth, Parts A/B/C*, *40–41*, 72–79. https://doi.org/10.1016/j.pce.2010.01.002.

Terranova, C., Ventura, G., & Vilardo, G. (2015). 'Multiple causes of ground deformation in the Napoli metropolitan area (Italy) from integrated Persistent Scatterers DinSAR, geological, hydrological, and urban infrastructure data'. *Earth-Science Reviews*, *146*, 105–119. https://doi.org/10.1016/j.earscirev.2015.04.001

Tiede, D., Krafft, P., Füreder, P., & Lang, S. (2017). 'Stratified template matching to support refugee camp analysis in OBIA workflows'. *Remote Sensing*, *9*(4), p. 326. https://doi.org/10.3390/rs9040326

Tukey, J. W. (1949). 'Comparing individual means in the analysis of variance'. *Biometrics*, *5*(2), 99–114. https://doi.org/10.2307/3001913

Uddin, M., Alam, J. B., Khan, Z. H., Jahid Hasan, G. M., & Rahman, T. (2014). 'Two dimensional hydrodynamic modelling of Northern Bay of Bengal coastal waters'. *Computational Water, Energy, and Environmental Engineering*, *3*(4), 140–151. https://doi.org/10.4236/cweee.2014.34015

Ul Haque, E. (2011) *'Survey of as yet un-surveyed parts of the Bangladesh coast to search for wintering shorebird concentrations (particularly Spoon-billed Sandpiper) and assess the hunting threats'*, *Bangladesh Oriental Bird Club* [Online]. (Retrieved October 15, 2019, from. https://static1.squarespace.com/static/5c1a9e03f407b482a158da87/t/5c252b280e2e72cac482659d/1545939753390/P920-Wintering-shorebirds-Bangladesh.pdf

Ullah, A. A. (2011). 'Rohingya refugees to Bangladesh: Historical exclusions and contemporary marginalization'. *Journal of Immigrant & Refugee Studies*, *9*(2), 139–161. https://doi.org/10.1080/15562948.2011.567149

Veci, L., Lu, J., Prats-Iraola, P., Scheiber, R., Collard, F., Fomferra, N., & Engdahl, M. (2014) 'The Sentinel-1 toolbox', *IEEE International Geoscience and Remote Sensing Symposium*. Quebec, Canada, 13-18 July 2014, 1–3.

Verjee, F. (2007) *An assessment of the utility of GIS-based analysis to support the coordination of humanitarian assistance*, Dissertation The George Washington University. Retrieved October 15, 2019, from. https://pqdtopen.proquest.com/pubnum/3297449.html

Villasenor, J., & Zebker, H. A. (1992) 'Temporal decorrelation in repeat-pass radar interferometry', *International Geoscience and Remote Sensing Symposium*. Houston, Texas, IEEE, 941–943.

Wei, M., Sandwell, D., & Smith-Konter, B. (2010). 'Optimal combination of InSAR and GPS for measuring interseismic crustal deformation'. *Advances in Space Research*, *46*(2), 236–249. https://doi.org/10.1016/j.asr.2010.03.013

Witmer, F. D. W., & O'Loughlin, J. (2011). 'Detecting the effects of wars in the Caucasus regions of Russia and Georgia using radiometrically normalized DMSP-OLS nighttime lights imagery'. *GIScience & Remote Sensing*, *48*(4), 478–500. https://doi.org/10.2747/1548-1603.48.4.478

Yang, Q., Ke, Y., Zhang, D., Chen, B., Gong, H., Lv, M., Zhu, L., & Li, X. (2018). 'Multi-scale analysis of the relationship between land subsidence and buildings: A case study in an eastern Beijing urban area using the PS-InSAR technique'. *Remote Sensing*, *10*(7), 1006. https://doi.org/10.3390/rs10071006.

Yu, C., Li, Z., Penna, N. T., & Crippa, P. (2018). 'Generic atmospheric correction model for interferometric Synthetic Aperture Radar observations'. *Journal of Geophysical Research: Solid Earth*, *123*(10), 9202–9222. https://doi.org/10.1029/2017JB015305